J Fluid Mech. (1976), *vol.* 78, *part* 4, *pp.* 689–707
Printed in Great Britain

A numerical simulation of the rarefied hypersonic flat-plate problem

By D. I. PULLIN AND J. K. HARVEY
Department of Aeronautics, Imperial College, London

(Received 3 February 1976)

The direct-simulation Monte-Carlo method for the full Boltzmann equation is applied to the problem of rarefied hypersonic flow of rotationally excited N_2 past the leading edge of a two-dimensional flat plate aligned with the free stream. An approximate collision model representing rotational–translational energy exchanges is developed for use in the calculations. The effects of this and other inelastic collision models and of the single-parameter Maxwell gas–surface interaction law on the flow in the kinetic/transition regime are discussed.

1. Introduction

The problem of hypersonic rarefied flow past a two-dimensional flat plate aligned with the free stream is one of fundamental interest since it generates a wide range of basic flow phenomena. These extend from a highly non-equilibrium kinetic flow near the leading edge through the merged layer and the strong and weak interaction regimes to a classical boundary-layer flow far downstream. But although the flow within and downstream of the merged layer is now well understood, a coherent experimental–theoretical picture of the initial kinetic region and the transition region has yet to emerge. On the experimental side it is widely recognized that, owing to the highly non-equilibrium nature of the flow in this region, accurate measurements are extremely hard to obtain. The problems of instrumentation and the large correction factors that must be applied to most readings, combined with the difficulties in establishing a uniform and precisely specified test flow, all contribute to the uncertainties in the results. On the theoretical side, progress towards accurate solutions for diatomic gases has been hampered for a variety of reasons. The most significant has been the formidable task of including the effects of rotational–translational energy exchange in numerical or other solutions of the Boltzmann equation which describes the kinetic flow at the molecular level. There is also uncertainty surrounding the precise gas–surface interaction law to be used in hypersonic situations. Neither of these two phenomena is properly understood, yet they have sizable effects on the development of the initial kinetic flow.

Several different approaches have been adopted in solving the leading-edge problem. Using finite-difference methods, Tannehill, Mohling & Rakich (1973) have attempted to extend the solution of the time-dependent Navier–Stokes equation, i.e. the continuum equation, into the kinetic regime by incorporating

velocity slip and a temperature jump at the wall. They have obtained unexpectedly plausible results, however, for $\gamma = 1{\cdot}4$ it is probable that the neglect of rotational non-equilibrium effects partially compensates for the inadequacy of the continuum equations upstream of the merged layer. A more rigorous approach has been made by Huang *et al.* (1972), who, following earlier work, have applied discrete ordinate methods to polyatomic extensions of BGK-type model equations and have obtained the first kinetic-theory treatment of the leading-edge problem for a diatomic gas. For a free-stream Mach number M_∞ of 6·1 these authors conclude that the presence of the rotational internal energy has a considerable effect on the structure of the flow field near the leading edge.

The methods of the above references yield reasonable results at moderate M_∞. However, since both employ approximations to the Boltzmann equation which are of dubious validity at high M_∞, it is difficult to justify their extension to the hypersonic situation.

The direct-simulation Monte-Carlo method (DSM), devised by Bird, yields numerical solutions for the full nonlinear Boltzmann equation (see Bird 1970*b*). It has already been successfully applied to the leading-edge problem for a monatomic gas by Bird (1966) and later, for very high M_∞, by Vogenitz, Broadwell & Bird (1969). A notable feature of these calculations is that, for plates at least several times the free-stream mean free path λ_∞ in length, the initial kinetic flow is not dominated by free molecular effects. This is contrary to Lewis's (1971) interpretation of his experimental data for a diatomic gas.

In theory the DSM may be applied to polyatomic gas flows provided that a model is available which incorporates the internal–translational energy exchange in inelastic collisions. Unfortunately simple impulsive models have proved unsuitable for simulation while the use of more realistic classical models (Macpherson 1971) such as that due to Parker (1959) or their quantum equivalents is not feasible for the treatment of complex flows because of prohibitive computing-time requirements. Recently several phenomenological/statistical collision models have been proposed (see Bird 1970*a*; Borgnakke & Larsen 1973; Larsen & Borgnakke 1974) which essentially trade a realistic microscopic description of the energy transfer process in return for simplicity and flexibility. As yet the development of such models has only just begun and their further refinement should provide powerful schemes for many applications to polyatomic gases.

In the present report we extend an earlier study (Pullin, Harvey & Bienkowski 1974) of direct-simulation calculations for the hypersonic two-dimensional leading-edge flow of a rotationally excited but vibrationally frozen diatomic gas. Emphasis is here placed on investigating some of the effects of using different binary collision models and gas–surface interactions on the flow in the kinetic regime and the subsequent transition to a merged-type flow. For the most part the calculations were performed using a hybrid collision model composed of an approximate form of Parker's classical soft-molecule model in conjunction with a two-class statistical technique due to Borgnakke & Larsen (1973). Calculations using the energy-sink method (Bird 1970*a*) and the restricted-exchange model (Larsen & Borgnakke 1974) are also presented.

2. The direct-simulation method

The direct-simulation Monte-Carlo method (Bird 1970*b*), the technique used in the present study, bypasses analytical formulations of kinetic theory in favour of a direct numerical probabilistic formulation of the full Boltzmann equation

$$\frac{\partial(nf)}{\partial t} + \mathbf{v}.\frac{\partial(nf)}{\partial \mathbf{x}} = \left[\frac{\partial(nf)}{\partial t}\right]_{\text{coll}} \tag{1}$$

from the calculated motion of several thousand sample particles. In (1), $f(\mathbf{x}, \mathbf{v}, E, t)$ is the distribution function, $\mathbf{x}$ the position vector, $\mathbf{v}$ the particle velocity, E the particle internal energy, $n(\mathbf{x}, t)$ the number density and the right-hand side represents the collision integral (see Chapman & Cowling 1970, chap. 3).

The simulation computes the time evolution of the sample ensemble in a bounded region of classical phase space ($\mathbf{x}$, $\mathbf{v}$, E space) from a specified initial configuration. A discretization of time into intervals $t_m \leqslant t \leqslant t_m + \Delta t_m$, $m = 1, 2, \ldots$, where Δt_m satisfies the convection and collision conditions

$$\bar{\mathbf{v}}.\Delta t_m/\Delta x \ll 1, \quad \Delta t_m \ll \tau_m, \tag{2}$$

$\bar{\mathbf{v}}$ being an average velocity and τ_m the local mean free time, allows the decoupling of the convection and collision terms in (1). Each may then be simulated alternately in the time-interval sequence independent of the other. During the convection mode particles move on free trajectories in the region of physical simulation space Ω and may either be lost from Ω across imaginary boundaries or may reflect from a solid boundary according to some prescribed surface interaction law. For the collision simulation, a statistical interpretation of the complete collision integral in (1) allows the formulation of binary collision probabilities per particle pair in a system of contiguous cells ω_k, $k = 1, \ldots, K$, of Ω. These, together with a time increment per collision

$$\Delta t_k = 2\Delta \mathbf{x}_k/\bar{\rho}_k N_k^2 g \pi b_0^2(g), \tag{3}$$

where $\Delta \mathbf{x}_k$ is the cell volume, N_k the number of particles in ω_k, $\bar{\rho}_k$ the real-to-simulated gas density ratio and $b_0(g)$ the maximum allowed impact parameter (miss distance), g being the pair's relative speed, ensures that collisions are simulated at the appropriate rate in each ω_k. The calculation is always unsteady, a steady flow existing in a stochastic sense where boundary conditions are such that a macroscopic steady flow would be expected after some transient time. Extensive experience with the DSM by several users indicates that it is all but unconditionally stable.

An important practical advantage of the method is that f need not be considered explicitly, the phase-space information being carried directly by the sample particles. Thus estimates of fluid state or surface flux properties are obtained by averaging the contributions of individual sample particles as they pass through cells or strike segments of a body surface. Any moment $\langle Q(\mathbf{v}, E)\rangle$ of f is then approximated by

$$\bar{Q} = \frac{1}{N}\sum_{n=1}^{N} Q_n \tag{4}$$

over a sample of N independent observations.

3. Collision model

The calculation of individual binary collisions and the subsequent replacement of the pre-collision dynamical co-ordinates by their post-collision values constitute an integral part of the DSM. A binary collision is defined by the initial relative translational energy $E_t = \frac{1}{4}mg^2$ of the pair's mass centre, the initial rotational energies E_i, $i = 1, 2$, the miss distance b and the azimuthal angle θ. The post-collision values of the energies are denoted by E_t' and E_i', $i = 1, 2$.

We assume that inelasticity affects collisions only through energy transfer superimposed on an otherwise spherical scattering process. Thus the pair conditional collision probability $P(g) \propto gb_0^2(g)$ and the deflexion angle $\chi_0(b, g)$ can be computed from monatomic collision dynamics independently of E_i, $i = 1, 2$.

Using the Morse potential

$$V_0(r) = 4kT_0[e^{-\alpha(r-\sigma)} - e^{-\frac{1}{2}(r-\sigma)}], \tag{5}$$

where T_0 is the attractive well depth temperature, α the range factor and $r = \sigma$ the potential zero point,† χ_0 was computed as a function of $(b/b_0)^2$ and $g^* = g(4kT_0/m)^{-\frac{1}{2}}$ by quadrature and stored as an array for use in the simulation. An arbitrary cut-off for χ_0 in $(b/b_0)^2$, g^* space was used to define the maximum miss distance $b_0(g^*)/\sigma$ such that the χ_0 singularities (see Hirschfelder, Curtiss & Bird 1954, p. 555) for $g^* \leqslant g_c^*$, the critical orbiting speed, were included. The range of g^* considered was 10·0–0·01 and the small number of collisions outside this were neglected. It is further assumed that molecular rotation is the only internal energy mode available for exchange with translational energy during collisions and that vibrational and other internal modes remain frozen.

Ideally a model of the inelastic exchange should (i) satisfy some form of detailed balancing principle (see Chapman & Cowling 1970, pp. 68, 204) necessary to obtain at equilibrium energy equipartition of $\frac{1}{2}kT$ per degree of freedom per molecule and the appropriate Boltzmann velocity and internal energy distributions and(ii) retain a realistic microscopic description of the inelastic exchange process. We regard this as important in the present context because of the large departures from equilibrium and the high degree of anisotropy in the initial kinetic leading-edge flow.

There is evidence based on transport-theory calculations (Lordi & Mates 1970) that an approximate analytical form of Parker's (1959) non-spherical classical potential model retains some physical features of the exchange process, but owing to simplifications and approximations employed, detailed balance is violated. On the other hand a simple relaxation technique proposed recently (Borgnakke & Larsen 1973) which incorporates a purely statistical two-class model of the energy exchange satisfies detailed balancing but is probably unrealistic far from equilibrium. For the present calculations we have adopted a hybrid approach in which the energy exchange is treated either classically or statistically in an *ad hoc* fashion described below. The composite model is constructed in a manner which retains some advantages of either approach.

† For N_2, $T_0 = 91{\cdot}5$ °K, $\alpha = 4{\cdot}02$ Å^{-1}, $\sigma = 3{\cdot}81$ Å and $g_c^* = 1{\cdot}23$.

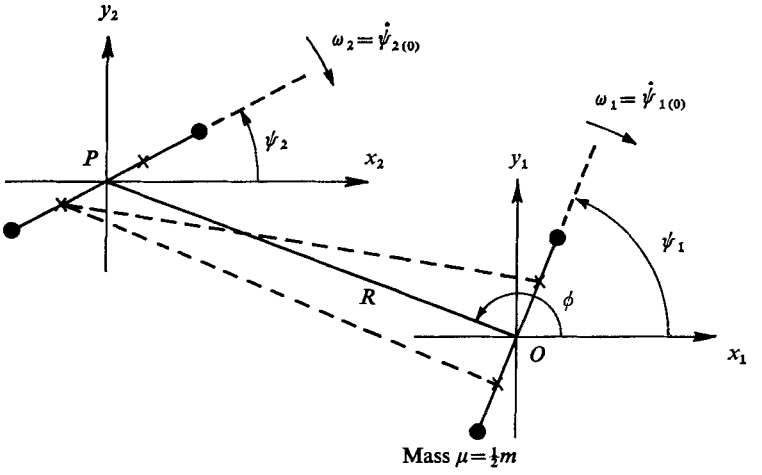

FIGURE 1. Molecular orientation for planar rotation.

The classical method, originally due to Parker (1959), is based on perturbation methods and leads to an approximate analytical solution for the energy transfer per particle in terms of the pre-collision dynamical and geometrical co-ordinates.

Parker (1959) and Lordi & Mates (1970) consider the collision of two identical homonuclear rigid rotor molecules, assuming that the rotation plane of each coincides with the collision plane (coplanar collisions). The interaction potential is the modified Morse model, given for this case by

$$V(r) = V_0(r) + \delta V_1(r, \phi, \psi_1, \psi_2), \tag{6}$$

where

$$V_1(r, \phi, \psi_1, \psi_2) = 4kT_0 e^{-\alpha(r-\sigma)} \sum_{i=1}^{2} \cos[2(\phi - \psi_i)], \tag{6a}$$

ϕ and ψ_i, $i = 1, 2$ are as in figure 1 and δ represents the potential non-sphericity. The Parker solution proceeds by assuming $\delta \ll 1$ and expanding the solution in the form

$$\left.\begin{aligned} r(t) &= r_0(t) + \delta r_1(t) + \delta^2 r_2(t) + \ldots, \\ \phi(t) &= \phi_0(t) + \delta\phi_1(t) + \delta^2\phi_2(t) + \ldots, \\ \psi_i(t) &= \psi_{i0}(t) + \delta\psi_{i1}(t) + \delta^2\psi_{i2}(t) + \ldots, \quad i = 1, 2. \end{aligned}\right\} \tag{7}$$

Substitution of (7) into the Lagrangian form of the equations of motion leads to zeroth-, first- and higher-order perturbation equations for the system. The solution $\psi_{i0}(t)$ is simply that for steady rotation:

$$\psi_{i0}(t) = \omega_i t + \gamma_i, \tag{8}$$

where $\pi \geqslant \gamma_i \geqslant 0$ is the rotor orientation at the point of closest approach ($t = 0$) and $\omega_i = \dot{\psi}_{i0}(-\infty)$ is the initial angular velocity, at $t = -\infty$. The energy transfer is

$$\overline{\Delta E_i} = \bar{E}_i' - E_i = \delta I \omega_i \overline{\dot{\psi}_{i1}}(\infty) + \tfrac{1}{2} I \delta^2 [\overline{\dot{\psi}_{i1}^2}(\infty) + 2\omega_i \overline{\dot{\psi}_{i2}}(\infty)] + O(\delta^3), \quad i = 1, 2, \tag{9}$$

where $I = \frac{1}{4}md^2$ is the moment of inertia of a rigid rotor molecule, m is the

molecular mass, d the internuclear separation and $E_i = \frac{1}{2}I\omega_i^2$ is the initial rotational energy. The bars in (9) refer to averages over γ_i uniformly distributed in $(0, \pi)$.

Using an approximate solution for $r_0(t)$, Lordi & Mates [1970, equation (44)] obtain a closed-form solution for $\psi_{i1}(\infty)$. It turns out that $\overline{\psi_{i1}}(\infty)$ vanishes but that $\overline{\psi_{i1}^2}(\infty)$ is finite. However, from (9) we see that, for consistency to order δ^2, an approximation to $\overline{\psi_{i2}}(\infty)$ is required, which means considering the second-order rotational equations. In the appendix, a solution of this kind is obtained, namely (32). Substituting this together with the equation [(31) from the appendix] for $\overline{\psi_{i1}^2}(\infty)$ into (9) we find an expression for the orientation-averaged energy exchange:

$$\Delta E_i = \delta^2(kT_0)\,(2/\alpha d)^2 x^6\, F_1(F_1 - 2z' F_2), \quad i = 1, 2, \tag{10}$$

where

$$F_1(x,z) = \int_{-\infty}^{\infty} \frac{\cos(uz)\,du}{[(1+x^2)^{\frac{1}{2}}\cosh u - 1]^2}, \quad F_2(x,z) = \int_{-\infty}^{\infty} \frac{u\sin(uz)\,du}{[(1+x^2)^{\frac{1}{2}}\cosh u - 1]^2}$$

and

$$x = \xi/(4RT_0)^{\frac{1}{2}}, \quad \xi = g[1-\hat{b}^2]^{\frac{1}{2}}, \quad \hat{b} = b/\sigma,$$

$$z' = (8/\alpha d)\,(\bar{E}_i/2kT_0)^{\frac{1}{2}} x^{-1}, \quad z = z' - (4/\alpha\sigma)\,\hat{b}(1-\hat{b}^2)^{-\frac{1}{2}}.$$

The integrals F_1 and F_2 may be evaluated by contour integration, which leads to an expression for $\overline{\Delta E_i}$ in terms of a few elementary functions. However, (10) is not suitable for all classes of collisions. By considering an extreme case of initially non-rotating ($E_i = 0$) head-on collisions ($b = 0$), then using (10) and evaluating $F_1(x, 0)$, it may be shown that the ratio of the energy transferred to the initial translational energy is

$$(\overline{\Delta E_1} + \overline{\Delta E_2})/E_t = 2(4\delta/\alpha d)^2\,[(\pi + x - \tan^{-1}x)/x]^2, \tag{11}$$

where here $x = E_t/kT_0$. Clearly this ratio must be less than unity but for N_2, using Parker's values of $d = 1{\cdot}09$ Å and $\delta = 0{\cdot}259$,† the left-hand side of (11) is equal to 0·45 for $x = 2$ and exceeds unity for $x \lesssim 1{\cdot}2$. Thus (10) cannot be uniformly valid for values of E_t characteristic of collisions at equilibrium temperatures T_0 or lower, most probably because the expansion (7) fails to converge. Furthermore, even for temperatures $T \gg T_0$, when (10) is used in a simulation it does not lead to complete energy equipartition at equilibrium. This may be attributed to violation of detailed balancing (the lack of inverse collisions) due in turn to the assumptions employed in developing the model, particularly that of coplanar collisions.

Using the relaxation technique (Borgnakke & Larsen 1973), for given E_t and E_i ($i = 1, 2$), E_t' and E_i' ($i = 1, 2$) are computed in a statistical manner assuming a two-class transfer. Collisions are either fully elastic with probability $1/Z_R$ or fully inelastic with probability $(Z_R - 1)/Z_R$, Z_R being the constant pre-specified rotational collision number. For the elastic case, the post-collision probability distributions are constructed specifically to satisfy detailed balance. A possible

† See Lordi & Mates (1970). This value was obtained by matching predicted and experimental values of the rotational relaxation number Z_R for N_2. Both theory and experiment yield values of Z_R varying from $Z_R \simeq 2$ at $T = 100$° K to $Z_R \simeq 10$ at $T = 1000$ °K.

objection to the global use of this model for highly non-equilibrium situations was stated earlier.

In view of the shortcomings of both of the above techniques most of the calculations presented were performed using a hybrid approach where the classical Parker model is chosen for the collisions of high relative translational energy and the statistical method for low energy encounters as follows.

(i) If $E_t < 2kT_0$, E_t' and E_i' $(i = 1, 2)$ are calculated using the Borgnakke & Larsen model with $Z_R = 3$.

(ii) If $E_t \geqslant 2kT_0$ the classical model is chosen. Equation (10) is used to determine $\Delta E_i'$ $(i = 1, 2)$ then E_t' is computed from $E_t' = E_t - (\Delta E_1 + \Delta E_2)$.

(iii) If (ii) leads to an exchange which drives the pair internal energy towards a state of two-particle energy equipartition (defined by $E_1 = E_2 \simeq \frac{1}{2}E_t$ for two internal degrees of freedom), then the classical transfer is accepted. If not the transfer is recalculated using the relaxation model.

The above technique is purely *ad hoc*, designed essentially to drive the gas into a state of local energy equipartition in a manner similar to the energy-sink method (Bird 1970*a*) while retaining, far from equilibrium, for $E_t > 2kT_0$, a detailed description of the energy exchange process with a correlation between the pre- and post-collision properties. The model correctly simulates temperature relaxation and has been shown to lead to approximate energy equipartition at equilibrium for temperatures up to 2000 °K. Note that this is not automatically guaranteed since an H-theorem cannot be established. At equilibrium, the velocity distribution is Maxwellian but the correct $\exp(-E_i/kT)$ rotational energy distribution is not achieved.

4. Boundary conditions

The physical simulation space Ω is bounded by $\partial\Omega_2$, the solid body surface, and $\partial\Omega_1$, an arbitrary curve within the fluid. On $\partial\Omega_1$, the incident boundary condition is taken to be free-molecule flow of the free stream. Thus at each Δt_m a nearly fixed number of sample particles, determined by the simulated free-stream density, enters Ω along $\partial\Omega_1$, their dynamical properties being sampled from the distribution

$$f_+ \propto \mathbf{v}.\mathbf{n} \exp\{-[\tfrac{1}{2}m(\mathbf{v}-U_\infty)^2 + E]/kT_\infty\} \quad \text{for} \quad \mathbf{v}.\mathbf{n} > 0, \tag{12}$$

where $\mathbf{n}$ is the inward normal to $\partial\Omega_1$. For $\mathbf{v}.\mathbf{n} < 0$ the boundary condition is automatically satisfied by particles leaving Ω during the convection simulation mode.

The boundary condition on $\partial\Omega_2$ was taken to be the Maxwell gas–surface law specified by the surface reflexion kernel (see Kuščer 1974)

$$P(\mathbf{v}, E|\mathbf{v}', E') \propto (1-\sigma')\,\delta(\mathbf{v}'-\mathbf{v}_R')\,\delta(E'-E) + \sigma'(2/\pi)\,\mathbf{v}'.\mathbf{n} \exp\{-(\tfrac{1}{2}mv'^2 + E')/kT_w\}, \tag{13}$$

where T_w is the wall temperature, i.e. we assume a combination of specular reflexion with probability $1-\sigma'$ and fully diffuse, fully accommodated reflexion at T_w with probability σ'. The three values of σ' chosen for the calculations were $\sigma' = 0{\cdot}5$, $0{\cdot}75$ and $1{\cdot}0$.

M_∞	T_∞ (°K)	T_w/T_∞	γ	Collision model	$Q^{(2)*}$	$\lambda_\infty/\lambda_{fb}$	σ'	L/λ_∞
21	20·0	14·4	$\frac{5}{3}$	Morse potential	0·83	0·073	1·0	96
22·93	20·0	14·4	$\frac{7}{5}$	Morse + hybrid model	0·83	0·073	1·0	96
22·9	—	14·4	$\frac{7}{5}$	$\alpha = 8$.† Energy sink	—	0·068	1·0	100
22·9	—	14·4	$\frac{7}{5}$	$\alpha = 13{\cdot}55$† Statistical	—	0·103	1·0	100
25	10·0	30	$\frac{7}{5}$	Morse + hybrid model	0·79	0·048	1·0	102
25	10·0	30	$\frac{7}{5}$	Morse + hybrid model	0·79	0·048‡	0·75	204
25	10·0	30	$\frac{7}{5}$	Morse + hybrid model	0·79	0·048‡	0·50	306

† α = exponent in inverse power law $V = a/r^\alpha$.
‡ Note, these values of $\lambda_\infty/\lambda_{fb}$ assume $\sigma' = 1$.

TABLE 1. Flow conditions

5. Flow conditions

The flow conditions used for the calculations were chosen to match those of recent N_2 experiments (Lewis 1971; J. Davis 1974, private communication) at $M_\infty \simeq 20$–25 and are summarized in table 1. Each plate was of finite length L and had a sharp leading edge (at the origin of Cartesian co-ordinates (x, y) with x positive in the flow direction) with a 10° undersurface angle. The upstream portions of $\partial\Omega_1$ were tailored to contain forward propagation effects from the undersurface in so far as these may influence the flow for $y > 0$.

In simulations the length unit was $\lambda_\infty = 2\eta(T_\infty)/\rho\bar{c}$, where $\bar{c} = (8RT_\infty/\pi)^{\frac{1}{2}}$ and $\eta(T_\infty)$ is the viscosity for the chosen collision model. However, for many kinetic flow situations λ_∞ is not a suitable length scale, first since it is rather too sensitive to the collision model at the low free-stream temperatures at which experiments are performed and secondly since it does not relate directly to any limiting physical model of the flow. More widely used length scales based on the free-molecule limit are the free-stream and body-reflected particle free paths λ_{fb} and λ_{bf} respectively (Hamel & Cooper 1969). For $\sigma' = 1$ we take these to be

$$\lambda_{fb} = \frac{(T_w/T_\infty)^{\frac{1}{2}}}{n_\infty \pi\sigma^2 Q^{(2)*}(g^*)}, \quad \lambda_{bf} = \frac{\lambda_{fb}}{S_\infty}, \tag{14}$$

where $Q^{(2)*}$, a function of speed, is a standard collision integral associated with the viscosity cross-section (see Hirschfelder *et al.* 1954, §§82–84) for collisions between free-stream and typically diffusively body-reflected particles,

$$S_\infty = U_\infty/(2RT_\infty)^{\frac{1}{2}}$$

is the speed ratio, U_∞ is the free-stream speed and n_∞ the free-stream number density. For hard-sphere molecules $Q^{(2)*} = 1$. For the Morse potential we may take values for the similar Lennard Jones 6–12 model tabulated in Hirschfelder *et al.* (1954, table I–R and (8.2–13).

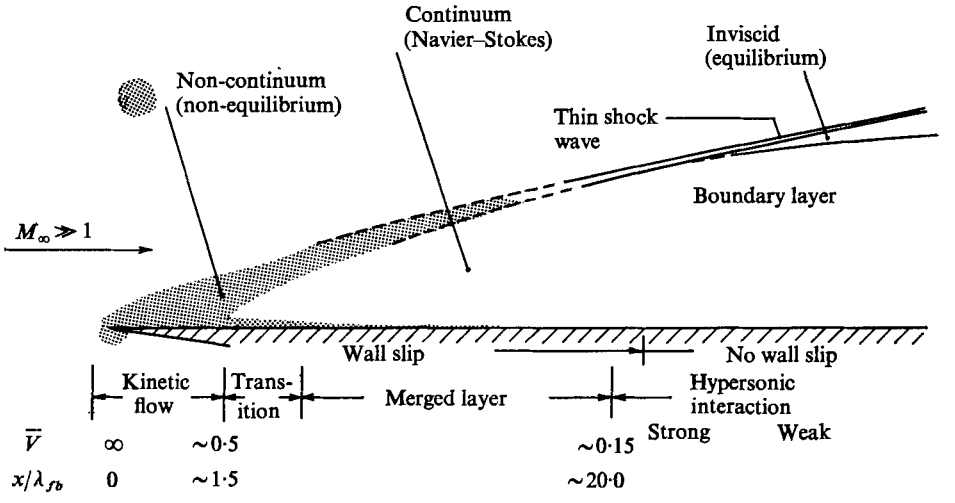

FIGURE 2. Schematic model of leading-edge flow.

Note that for $\sigma' < 1$ the above definitions of λ_{fb} and λ_{bf} must be modified by factors of $1/\sigma'$ and $\sigma'/(2-\sigma)$ respectively.

6. Results and discussion

Figure 2 shows a schematic representation of the flat-plate flow. Very near the leading edge collisions between free-stream and body-reflected particles generate the initial kinetic disturbance. The highly non-equilibrium flow is here characterized by the strongly competing effects of molecule–molecule and molecule–body encounters and the distribution function is far from Maxwellian. Further downstream molecule–molecule collisions begin to dominate, causing a transition to an essentially continuum flow in which the initial disturbance develops the dual features of a wall boundary layer merged with a non-Rankine–Hugoniot shock. The fully continuum strong and weak interaction regimes which develop even further downstream are outside the range of the present calculations.

Earlier calculations (Pullin *et al.* 1974) for the case $\sigma' = 1$ indicated the following.

(i) The initial collisional disturbance extends forward of the leading edge with the result that some surface properties exceed the free-molecule limit as $x \to 0^+$.

(ii) The transition to a merged-layer type of flow begins near $x/\lambda_{fb} \simeq 1$ and is accompanied by maxima in the surface flow properties.

(iii) Through energy absorption in initial collisions, the rotational degrees of freedom cause substantial quantitative changes in the flow properties compared with the monatomic case.

Figures 3–9 show a selection of flow properties obtained from the present calculations using estimates of the type (4). It is generally assumed that, for N large in (4), each $\bar{Q}$ is normally distributed with mean $\langle Q \rangle$ and relative standard

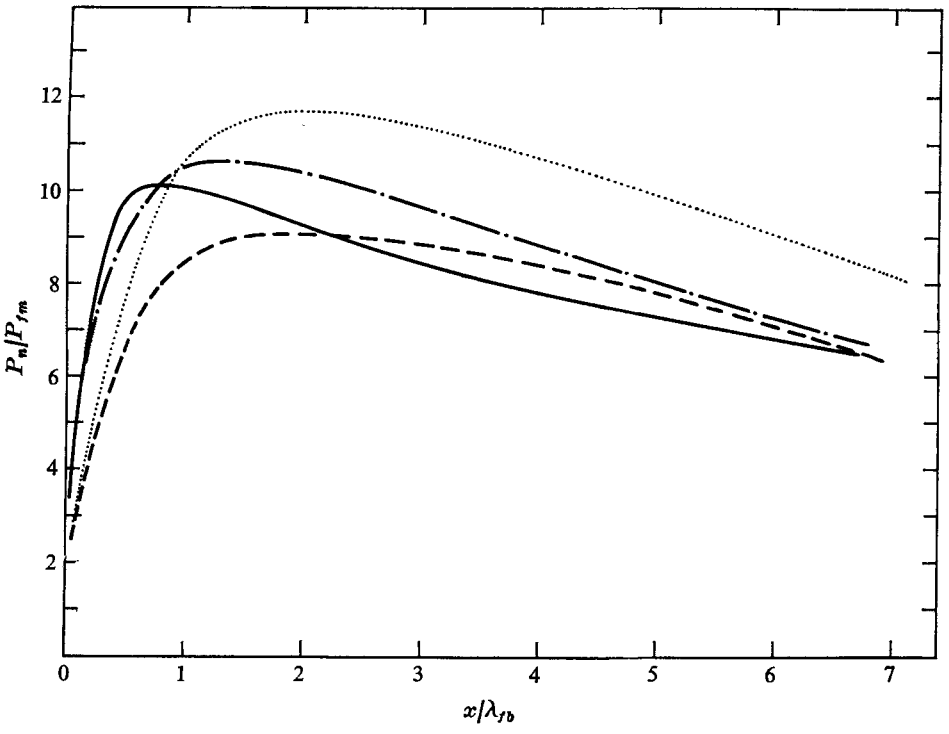

FIGURE 3. Effect of molecular model on the plate pressure. $M_\infty = 22{\cdot}93$, $T_w/T_\infty = 14{\cdot}4$, $\sigma' = 1$. ····, monotomic model with Morse potential; – – –, present diatomic model. Inverse-power law, $V_0(r) = a/r^\alpha$: ——, $\alpha = 8$, energy-sink model; — · —, $\alpha = 13{\cdot}5$, restricted-energy-exchange statistical model.

deviation $\bar{S}/\bar{Q} \simeq N^{-\frac{1}{2}}$. Hence for 3% relative deviation, $N \sim 10^3$ is required, which was generally the value obtained in the present calculations. In the figures, where the interests of clarity permit, actual calculated points have been plotted so as to give a ready indication of scatter in the results.

Figure 3 shows, for $\sigma' = 1$, the normal surface pressure P_n/P_{fm} calculated using different molecular models. The free-molecule pressure P_{fm} is defined later in (15). These models include the present hybrid model together with Bird's (1970*a*) energy-sink method and the restricted-energy-exchange statistical method (Larsen & Borgnakke 1974), both for inverse-power-law potentials. Also shown is the result of a monatomic calculation using the spherical Morse potential, which, when compared with that for the present diatomic model, indicates that the energy-absorbing effect of the rotational degrees of freedom leads to a reduction in the pressure peak. The results for the three diatomic models show significant agreement for $x/\lambda_{fb} > 3$ but there are rather large discrepancies in the kinetic/transition regimes, which may be due to several factors. First, the inverse-power models are purely repulsive and do not include an attractive potential well as does the Morse model. We may expect this to have some effect in the present problem since $T_\infty \ll T_0$. That this is so may be seen by noting that, for small x/λ_{fb}, P_n/P_{fm} for the inverse-power-law diatomic models

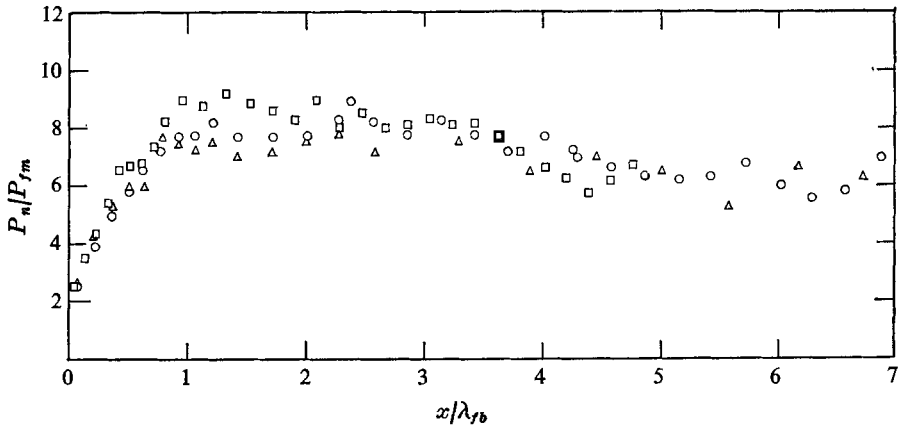

FIGURE 4. Plate pressure. $M_\infty = 25$, $T_w/T_\infty = 30$.
□, $\sigma' = 1{\cdot}00$; ○, $\sigma' = 0{\cdot}75$; △, $\sigma' = 0{\cdot}50$.

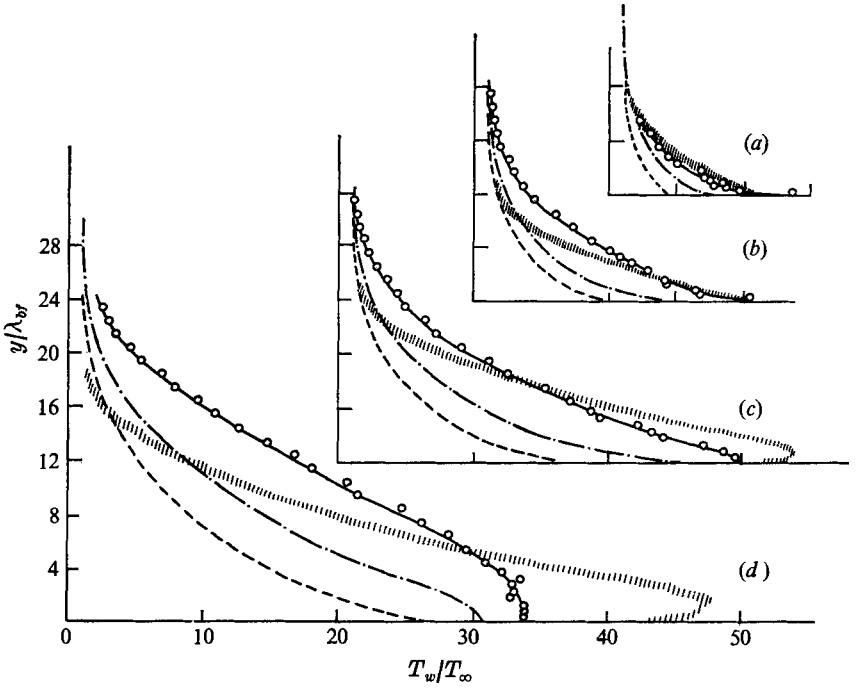

FIGURE 5. Rotational temperature profiles. $M_\infty = 25$, $T_w/T_\infty = 30$. ▥, data, Lewis (1971). Calculations: —○—, $\sigma' = 1{\cdot}00$; —·—, $\sigma' = 0{\cdot}75$; – – –, $\sigma' = 0{\cdot}50$. (*a*) $x/\lambda_{fb} = 0{\cdot}24$. (*b*) $x/\lambda_{fb} = 0{\cdot}70$. (*c*) $x/\lambda_{fb} = 1{\cdot}30$. (*d*) $x/\lambda_{fb} = 2{\cdot}70$.

exceeds the monatomic prediction. This is opposite to the expected influence of the internal degrees of freedom alone. A second effect related to the above is that, for large classes of important collisions, the present model accounts for the possible influence of anisotropy in the energy exchange process (first collisions have a highly preferred direction) and also for the effective variation of the rotational collision number with temperature.

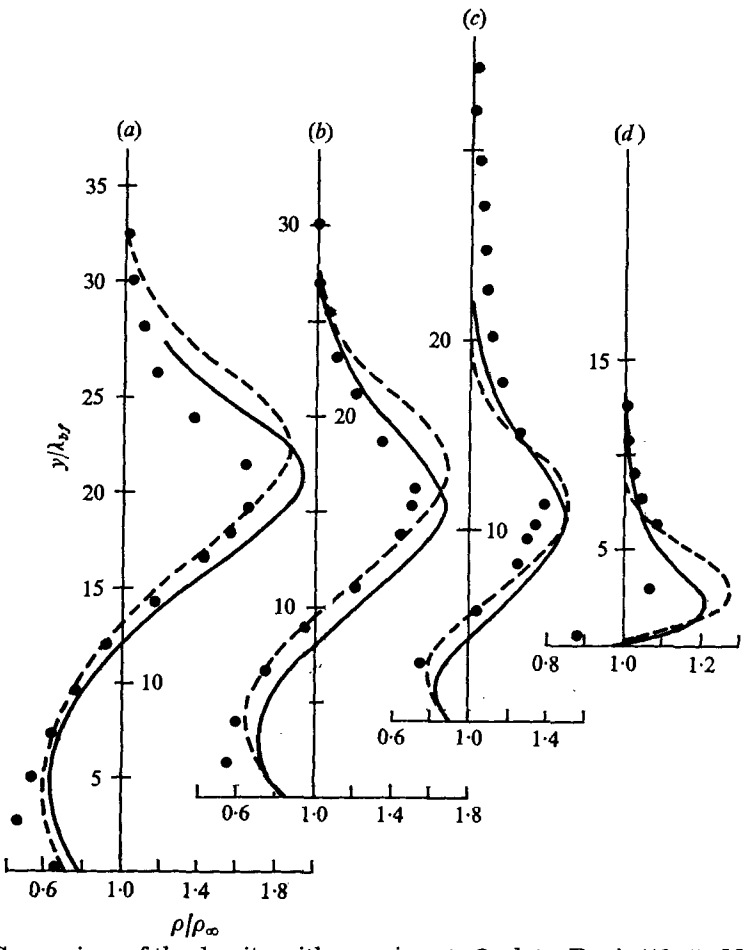

FIGURE 6. Comparison of the density with experiment. ●, data, Davis (1974), $M_\infty = 20{\cdot}56$, $T_w/T_\infty = 11{\cdot}4$. Present calculations for $M_\infty = 22{\cdot}93$, $T_w/T_\infty = 14{\cdot}4$: ——, hybrid collision model; – – –, statistical model, $\alpha = 13{\cdot}55$, $\phi = 0{\cdot}10$. (*a*) $x/\lambda_{fb} = 5{\cdot}9$. (*b*) $x/\lambda_{fb} = 4{\cdot}4$. (*c*) $x/\lambda_{fb} = 2{\cdot}8$. (*d*) $x/\lambda_{fb} = 0{\cdot}75$.

In figure 4 we have plotted P_n/P_{fm}, where the free-molecule pressure P_{fm}/P_∞ is

$$P_{fm}/P_\infty = \tfrac{1}{2}[(2-\sigma') + \sigma'(T_w/T_\infty)^{\frac{1}{2}}], \tag{15}$$

against x/λ_{fb} for the three values of σ'. Note that here λ_{fb} includes the σ' dependence indicated earlier with respect to (14). As can be seen, within the limits of statistical scatter, the three calculations collapse quite well onto a single curve in the kinetic regime upstream of the pressure peaks. If pressure is plotted as P_n/P_∞ then a factor of 100 % between the peaks for $\sigma' = 0{\cdot}5$ and $\sigma' = 1{\cdot}0$ results while if x/λ_∞ (or x/λ_{fb} for $\sigma' = 1$) is used as a horizontal scale there is a small but discernible separation of the results for the different cases.

Lewis (1971) measured the rotational temperature T_R directly throughout a hypersonic flat-plate flow field using an electron-beam technique. These measurements were extremely difficult to perform and Lewis, perhaps optimistically, considers them accurate to 2 % for $T_R \gtrsim 100\,°\text{K}$ with the error increasing to

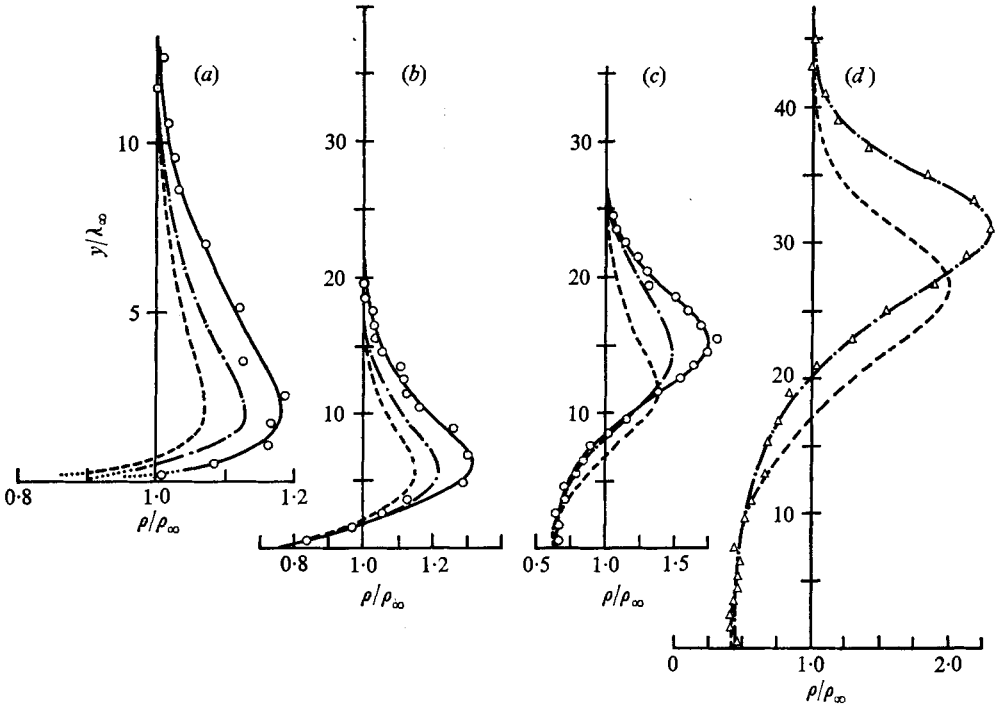

FIGURE 7. Effect of surface law on density. $M_\infty = 25$, $T_w/T_\infty = 30$. —○—, $\sigma' = 1{\cdot}0$; —·—, $\sigma' = 0{\cdot}75$; – – –, $\sigma' = 0{\cdot}50$. (*a*) $x/\lambda_\infty = 9$. (*b*) $x/\lambda_\infty = 27$. (*c*) $x/\lambda_\infty = 63$. (*d*) $x/\lambda_\infty = 150$.

about 40 % for $T_R \simeq 10\,^\circ\mathrm{K} = T_\infty$. Calculated rotational temperature profiles for three values of σ' at $T_w/T_\infty = 30$ are compared in figure 5 with Lewis's measured profiles. Agreement with the case $\sigma' = 1$ for $x/\lambda_{fb} \simeq 0{\cdot}24$ is quite good but becomes progressively worse further downstream. While this must be partly due to the approximate form of the present energy exchange model, there was almost certainly an axially decreasing free-stream temperature in the experiment which might contribute to the discrepancy downstream. Reducing the fraction of diffuse reflexion decreases the value of T_R throughout the flow field although for values of x/λ_{fb} larger than those shown this effect diminishes significantly near the wall. On the whole, the best agreement with the data is obtained for the fully diffuse case.

In figure 6 the calculated density profiles for two collision models (with $\sigma' = 1{\cdot}0$) are compared with the electron-beam data of Davis (1974, private communication). In general the near-surface behaviour of the experimental profiles and the position of the density peaks are quite well predicted by both calculations, but the density maxima are somewhat overestimated.

The effect of σ' on density at three x stations is shown in figure 7. Here we have used λ_∞ as the length scale as it is identical for all three cases. For the two upstream stations (in the kinetic regime) the effect of decreasing σ' is to reduce the density peak and this may be interpreted as a direct consequence of the diminished flux of diffusely reflecting particles convecting into the passing free stream.

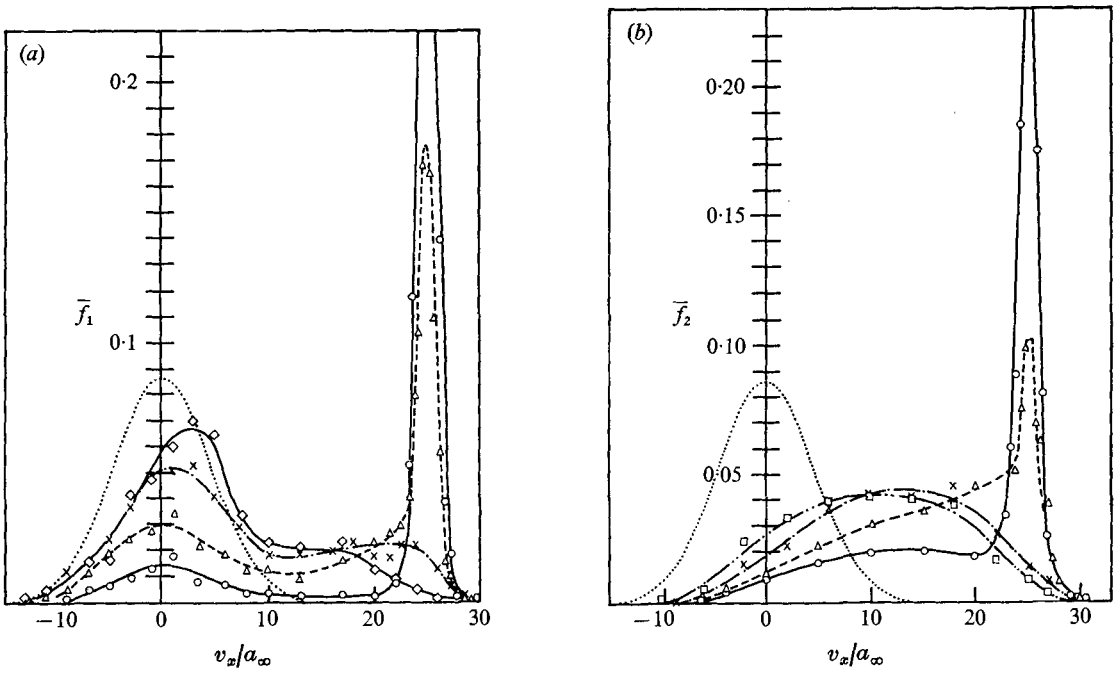

FIGURE 8. v_x distributions (*a*) near the wall and (*b*) for incident particles $M_\infty = 25, T_w/T_\infty = 30, \sigma' = 1{\cdot}0$. ·····, Maxwellian distribution. ○, $x/\lambda_\infty = 1$, $x/\lambda_{fb} = 0{\cdot}048$; △, $x/\lambda_\infty = 11$, $x/\lambda_{fb} = 0{\cdot}526$. (*a*) ×, $x/\lambda_\infty = 33, x/\lambda_{fb} = 1{\cdot}582$; ◇, $x/\lambda_\infty = 88, x/\lambda_{fb} = 4{\cdot}206$. (*b*) ×, $x/\lambda_\infty = 40$, $x/\lambda_{fb} = 1{\cdot}192$; □, $x/\lambda_\infty = 72, x/\lambda_{fb} = 3{\cdot}44$.

Further downstream, as the merged layer develops, the influence of σ' is mainly felt in the shock region as a legacy of that in the initial disturbance. In the lower part of the viscous layer, the near-surface flow approaches equilibrium with the wall and σ' plays a rapidly diminishing role.

In addition to macroscopic flow properties, estimates of reduced forms of the distribution function were also obtained from the calculations. These were of two kinds.

(i) The distribution of x velocities

$$\overline{f_1(v_x, x, y)} = \int_0^\infty \int_{-\infty}^\infty \int_{-\infty}^\infty f\, dv_y\, dv_z\, dE \tag{16}$$

in a number of spatial cells of Ω.

(ii) The reduced distribution of x velocities for particles striking segments of the plate surface (i.e. those with $v_y < 0$):

$$\overline{f_2(v_x, x)} = \frac{n}{N} \int_0^\infty \int_{-\infty}^\infty \int_{-\infty}^0 v_y f\, dv_y\, dv_z\, dE, \tag{17}$$

where n is the local number density and N the number flux per unit time incident on the segment.

Figure 8(*a*) shows histogram estimates of $\bar{f}_1$ obtained in four cells adjacent to the body surface for a calculation using the hybrid collision model and $\sigma' = 1{\cdot}0$. Figure 8(*b*) shows corresponding estimates of $\bar{f}_2$ for four nearby surface segments. Both figures illustrate the highly non-equilibrium character of the

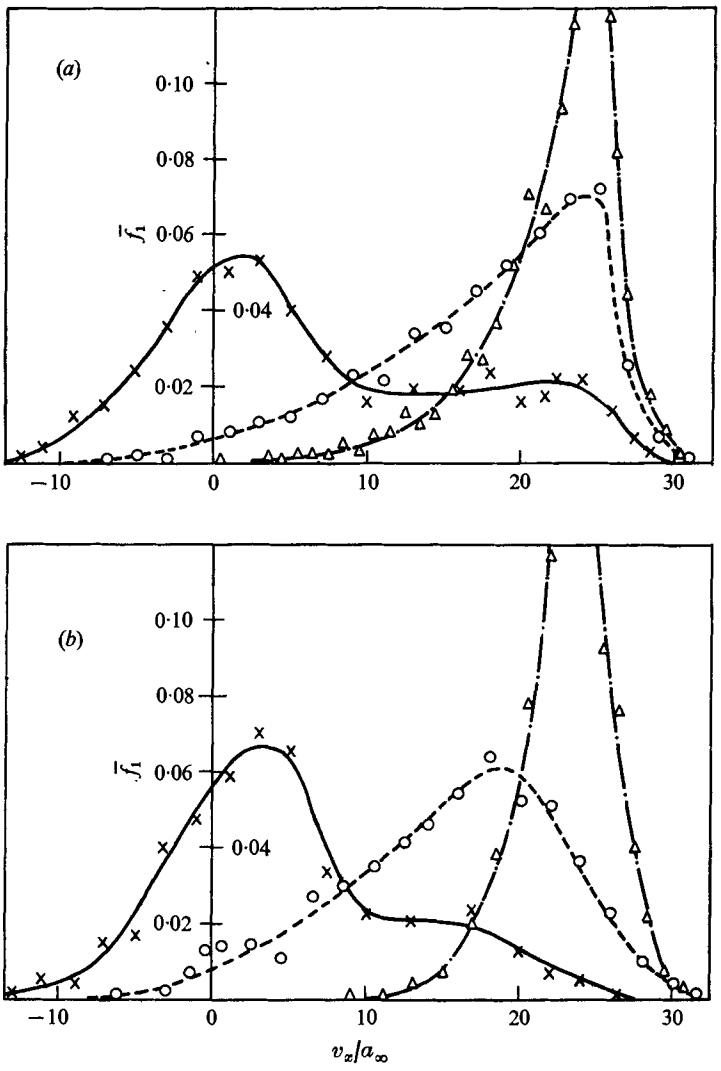

FIGURE 9. v_x distributions at (*a*) $x/\lambda_{fb} = 1{\cdot}58\,(x/\lambda_\infty = 33)$ and (*b*) $x/\lambda_{fb} = 4{\cdot}21$ $(x/\lambda_\infty = 88)$. $M_\infty = 25$, $T_w/T_\infty = 30$, $\lambda_{bf} = \lambda_\infty$. (*a*) ×, $y/\lambda_{bf} = 0{\cdot}25$; ○, $y/\lambda_{bf} = 3{\cdot}25$; △, $y/\lambda_{bf} = 7{\cdot}50$. (*b*) ×, $y/\lambda_{bf} = 0{\cdot}50$; ○, $y/\lambda_{bf} = 7{\cdot}50$; △, $y/\lambda_{bf} = 17{\cdot}50$.

distribution function for the near-surface flow. For $x/\lambda_{fb} = 0{\cdot}048$, $\bar{f}_1$ in figure 8 (*a*) gives the appearance of being typically free molecular with the tall narrow peak on the right representing the free stream and the squat peak near $v_x/a_\infty = 0$ the body-reflected particles. The sparsely populated band $10 \lesssim v_x/a_\infty \lesssim 20$, together with some particles in $v_x/a_\infty \lesssim 10$, represents collision products. However, the corresponding $\bar{f}_2$ in figure 8 (*b*) indicates that the flux of collision products to the surface is high in this region. Evidently, although the density of these particles is small, they have a high v_y and therefore greatly influence the surface flux properties near $x = 0$. Note that collision products for $x/\lambda_{fb} = 0{\cdot}048$ generally have $v_x > 0$, which means that they must have been created upstream

of this station. This supports the opinion that the initial collisional interaction between free-stream and body-reflected particles is significant in a region extending forward of the leading edge.

As the flow moves downstream the free-stream peaks for both $\bar{f}_1$ and $\bar{f}_2$ rapidly shrink owing to collisions. The broad $\bar{f}_2$ curves in figure 8(*b*) for $x/\lambda_{fb} = 1{\cdot}91$ and 3·44 show that at these stations a wide spectrum of slowly evolving incident collision products has developed while figure 8(*a*) clearly indicates the increasing importance of body-reflected particles in the near-surface flow. In particular the mixture of these and collision products is evident for $x/\lambda_{fb} = 1{\cdot}58$ and 4·21.

Figure 9 shows estimates of $\bar{f}_1$ obtained at various values of y/λ_{bf} for $x/\lambda_{fb} = 1{\cdot}58$ and 4·21. At both x stations the departures from a Maxwellian (equilibrium) v_x distribution appear to decrease for increasing y.

7. Conclusion

A direct numerical simulation of the rarefied hypersonic flow of a rotationally excited diatomic gas past the two-dimensional leading edge of a flat plate has been presented and in this context the effects of several inelastic collision models and of the Maxwell gas–surface law on the kinetic/transition regime flow have been investigated. For the chosen flow conditions with $T_\infty \ll T_0$ the collision models employed appear to have a considerable quantitative effect on the flow properties, particularly the plate normal pressure, in the kinetic/transition flow. This is attributed to the effect of the potential well present for the Morse potential but absent for the inverse-power-law models and also to the different treatment of rotational–translational energy exchange in elastic collisions. The influence of the collision model decreases as the merged layer forms, presumably since here the flow is in a more nearly equilibrium state with gas temperatures near the wall considerably exceeding T_0. The collision model used in the majority of the present calculations has been developed as an attempt to produce a realistic representation of the inelastic collision dynamics, which are thought to be important in the highly anisotropic (in velocity space) kinetic regime of the flat-plate flow. However, it suffers from a theoretical disadvantage in that detailed balance is not satisfied, a property which is hoped to be unimportant in the present calculations.

The calculations also indicate that a substantial portion of specular reflexion at the surface significantly affects the flow well into the merged layer, in agreement with the conclusions of Vogenitz *et al.* (1969) for the case of a monatomic gas. There is evidence (Kuhlthau & Bishara 1965) that the fully diffuse ($\sigma' = 1$) case is realistic for 'engineering' surfaces and by and large comparison of our results with available experimental data confirms this conclusion. We note, however, that the Maxwell model is a highly idealized one with the probability of specular reflexion being constant independent of particle incidence angle and energy. It has been suggested that fast particles approaching the plate at grazing incidence, say at angles of order $1/M_\infty$, may in some measure reflect specularly. If this were the case then a significant change in the flow properties over the first λ_{fb} could result which would be masked near the plate surface further downstream.

For reasons outlined briefly in the introduction it seems fair to say that at present a self-consistent, reliable and unambiguous body of measurements upstream of the merged layer is still lacking. It is therefore difficult to evaluate the results of the present calculations objectively, particularly for $x/\lambda_{fb} < 1$, by direct comparison with experiment. Judging by the sparse evidence shown in figure 6, both the hybrid collision model and the statistical model overpredict the density in this region, the latter by a greater margin. In the authors' view, further and more accurate flow measurements in the kinetic regime are a prerequisite for any worth-while development of the present technique applied to the flat-plate problem.

The authors wish to thank Professor G. A. Bird, who kindly supplied his 'Universal' program, with which the energy-sink and restricted-exchange model calculations were performed. This program was also used to check other results presented herein obtained using the authors' own programs. The research was sponsored by the Science Research Council.

Appendix

The Lagrangian form of the rotational equations of motion for the planar rotation case are

$$I\ddot{\psi}_i = -\partial V/\partial\psi_i, \quad i = 1, 2. \tag{18}$$

Substituting the expansion for $\psi_i(t)$ in (7) and the expansion (6) for the potential into (18) and equating terms of second order in δ leads to the following equation for $\psi_{i2}(t)$:

$$\begin{aligned} I\ddot{\psi}_{i2} = &-\psi_{i1}[\partial^2 V_1/\partial\psi_i^2]_0 - \psi_{j1}[\partial^2 V_1/\partial\psi_j\,\partial\psi_i]_0 \\ &-\phi_1[\partial^2 V_1/\partial\phi\partial\psi_i]_0 - r_1[\partial^2 V_1/\partial r\partial\psi_i]_0, \quad (i,j) = (1,2),(2,1). \end{aligned} \tag{19}$$

A complete solution to (19) first requires solutions of the first-order equations for $\psi_{i1}(t)$, $\phi_1(t)$ and $r_1(t)$ (the $\psi_{j1}\partial^2 V_1/\partial\psi_j\,\partial\psi_i$ term can be shown to vanish), which would be difficult to obtain. There is reason to believe, however, that the physical characteristics of a more complete solution, in particular a description of rotational de-excitation collisions, are retained if (19) is approximated by

$$I\ddot{\psi}_{i2} = -\psi_{i1}[\partial^2 V_1/\partial\psi_i^2]_0, \quad i = 1, 2, \tag{20}$$

that is the r_1 and ϕ_1 terms are neglected. This assumption cannot be justified *a priori* since by virtue of the ordering we should expect all terms to be of equal magnitude, but has been introduced primarily to lead to a tractable second-order equation. For this reason the present second-order solution remains incomplete. Note however that since the $\overline{\psi_{i2}(\infty)}$ term in (9) is weighted by ω_i, and since for the rotational excitation collisions we expect to dominate the leading-edge problem $\omega_i \ll [\overline{\psi_{i1}^2(\infty)}]^{\frac{1}{2}}$, the second term in (9) is probably less important than the $\overline{\psi_{i1}^2(\infty)}$ term, in the present context.

Substituting (6a) into (20) and integrating over t in $(-\infty, \infty)$ we obtain the second-order rotational speed at $t = \infty$ as

$$\psi_{i2}(\infty) = \frac{16kT_0}{I}\int_{-\infty}^{\infty} \psi_{i1}(t)\exp\left[-\alpha(r_0-\sigma)\right]\cos\left[2(\phi_0-\psi_{i0})\right]dt. \tag{21}$$

Lordi & Mates (1970) have obtained approximate solutions for $r_0(t)$ and $\psi_{i1}(t)$ which may be written as

$$\exp\left[-\alpha(r_0-\sigma)\right] = \frac{x^4}{4[A\cosh(at)-1]^2}, \tag{22}$$

$$\psi_{i1}(t) = \frac{2kT_0}{I}x^4\int_{-\infty}^{t}\frac{\sin(2\delta_i+2\nu_i u)\,du}{[A\cosh(au)-1]^2}, \tag{23}$$

where $\quad A = (1+x^2)^{\frac{1}{2}}, \quad a = \frac{1}{2}\alpha\xi, \quad \delta_i = \gamma_i - \phi_0(0), \quad \nu_i = \omega_i - gb/\sigma^2$

and x and ξ are as defined for (10). Since by (22) $\exp\left[-\alpha(r_0-\sigma)\right]$ is an even function of t which has a maximum at $t = 0$ and decreases as $\exp\left[-\alpha\xi|t|\right]$ for large $|t|$, the major contribution to the integral in (21) may be seen to be that near $t = 0$, where for our purposes other terms may be expanded locally as Taylor series. Expansions about $t = 0$ for $\psi_{i1}(t)$ and $\phi_0(t)$ lead to

$$\psi_{i1}(t) = \psi_{i1}(0) + \dot{\psi}_{i1}(0)\,t + \ddot{\psi}_{i1}(0)\,t^2 + O(t^3), \tag{24}$$

$$\phi_0(t) = \phi_0(0) + gb\sigma^{-2}t + O(t^2), \tag{25}$$

where using (23) the polynomial coefficients in (24) may be obtained as

$$\psi_{i1}(0) = -\frac{8kT_0}{I}\int_{-\infty}^{0}\exp\left[-\alpha(r_0-\sigma)\right]t\sin(2\delta_i+2\nu_i t)\,dt, \tag{26}$$

$$\dot{\psi}_{i1}(0) = \frac{8kT_0}{I}\int_{-\infty}^{0}\exp\left[-\alpha(r_0-\sigma)\right]\sin(2\delta_i+2\nu_i t)\,dt, \tag{27}$$

$$\ddot{\psi}_{i1}(0) = \frac{8kT_0}{I}\exp\left[-\alpha(r_0(0)-\sigma)\right]\sin(2\delta_i), \tag{28}$$

where the exponential factors in each of the above expressions are given by (22).

Substituting (8) and (24)–(28) together with (22) into (21), expanding the various trigonometric factors, neglecting terms of order $t^3\cos(2\nu_i t)$, $t^2\sin(2\nu_i t)$ or higher powers of t and averaging the final result over γ_i uniformly distributed in $(0, \pi)$ leads to

$$\overline{\psi_{i2}}(\infty) = -\left(\frac{2kT_0}{I}\right)^2 x^8\int_{-\infty}^{\infty}\frac{\cos(2\nu_i t)\,dt}{[A\cosh(at)-1]^2}\int_{-\infty}^{\infty}\frac{t\sin(2\nu_i t)\,dt}{[A\cosh(at)-1]^2} \tag{29}$$

for the orientation-averaged second-order rotational speed. Extending the upper limit of integration in (23) to ∞, then squaring and averaging over γ_i yields the first term of order δ^2 in (9):

$$\overline{\psi_{i1}^2}(\infty) = \frac{1}{2}\left(\frac{2kT_0}{I}\right)^2 x^8\left[\int_{-\infty}^{\infty}\frac{\cos(2\nu_i t)\,dt}{[A\cosh(at)-1]^2}\right]^2. \tag{30}$$

The transformation $u = at$ in (29) and (30) leads to

$$\overline{I\dot{\psi}_{i1}^2}(\infty) = 2kT_0\left(\frac{2}{\alpha d}\right)^2 x^6 F_1^2(x,z), \tag{31}$$

$$\overline{I\dot{\psi}_{i2}}(\infty) = -kT_0\left(\frac{2}{\alpha d}\right)^2\left(\frac{8}{\alpha\xi}\right) x^6 F_1(x,z)\, F_2(x,z), \tag{32}$$

where F_1 and F_2 are as for (10).

REFERENCES

BIRD, G. A. 1966 Aerodynamic properties of some simple bodies in the hypersonic transition regime. *A.I.A.A. J.* **4**, 55.

BIRD, G. A. 1970*a* Numerical simulation of the Boltzmann equation. *Preprint Dept. Aero. Engng, Univ. Sydney.*

BIRD, G. A. 1970*b* Direct simulation of the Boltzmann equation. *Phys. Fluids*, **13**, 2676.

BORGNAKKE, C. & LARSEN, P. S. 1973 Statistical collision model for Monte-Carlo simulation of polyatomic gas. *Dept. Fluid Mech., Tech. Univ. Denmark, Lyngby Rep.* AFM 73–08 (June 1973).

CHAPMAN, S. & COWLING, T. G. 1970 *The Mathematical Theory of Non-Uniform Gases*, 3rd edn. Cambridge University Press.

HAMEL, B. B. & COOPER, A. L. 1969 A first collision theory of the hyperthermal leading edge problem. In *Rarefied Gas Dynamics* (ed. Trilling & Wachman), suppl. 5, vol. 1, p. 443. Academic.

HIRSCHFELDER, J. O., CURTISS, C. F. & BIRD, R. B. 1954 *Molecular Theory of Gases and Liquids.* Wiley.

HUANG, A. B., HWANG, P. F., GIDDENS, D. P. & STRINIVANAN, R. 1972 High speed leading edge problem. *School Aerospace Engng, Georgia Inst. Tech., Atlanta Preprint*, no. 30332.

KUHLTHAU, A. R. & BISHARA, M. N. 1965 On the nature of the surface interaction between inert gas molecules and engineering surfaces. In *Rarefied Gas Dynamics* (ed. de Leeuw), suppl. 3, vol. 2, p. 518. Academic.

KUŠČER, I. 1974 Phenomenology of gas–surface accommodation. In *Rarefied Gas Dynamics 9th Symp.*, vol. 2 (ed. Becker & Fiebig), paper E 1. Potz-Wahn: DFVLR Press.

LARSEN, P. S. & BORGNAKKE, C. 1974 Statistical collision model for simulating polyatomic gas with restricted energy exchange. In *Rarefied Gas Dynamics, 9th Symp.*, vol. 1 (ed. Becker & Fiebig), paper A 7. Potz-Wahn: DFVLR Press.

LEWIS, J. H. 1971 An experimentally determined model for the noncontinuum flow at the leading edge in a high speed ratio stream. *Dept. Aerospace Mech. Sci., Princeton Univ., Rep.* no. 954.

LORDI, J. A. & MATES, R. E. 1970 Rotational relaxation in nonpolar diatomic gases. *Phys. Fluids*, **13**, 291.

MACPHERSON, A. K. 1971 Rotational temperature profiles of shock waves in diatomic gases. *J. Fluid Mech.* **49**, 337.

PARKER, J. G. 1959 Rotational and vibrational relaxation in diatomic gases. *Phys. Fluids*, **2**, 449.

PULLIN, D. I., HARVEY, J. K. & BIENKOWSKI, G. K. 1974 Hypersonic leading edge flow of a diatomic gas by the direct simulation method. In *Rarefied Gas Dynamics, 9th Symp.*, vol. 1 (ed. Becker & Fiebig), paper D 5. Potz-Wahn: DFVLR Press.

TANNEHILL, J. C., MOHLING, R. A. & RAKICH, J. V. 1973 Numerical computation of the hypersonic rarefied flow near the sharp leading edge of a flat plate. *A.I.A.A. Paper*, no. 73-200.

VOGENITZ, F. W., BROADWELL, J. E. & BIRD, G. A. 1969 Leading edge flow by the Monte-Carlo direct simulation technique. *A.I.A.A. Paper*, no. 69–141.